JOURNAL OF GEOPHYSICAL RESEARCH, VOL. 103, NO. C4, PAGES 7735–7748, APRIL 15, 1998

Seasonal and interannual variability of surface photosynthetically available radiation in the Arabian Sea

Robert A. Arnone,[1] Sherwin Ladner,[2] Paul E. La Violette,[3]
John C. Brock,[4] and Peter A. Rochford[5]

Abstract. The regional and monthly intensity of photosynthetically available radiation (PAR) (350–700 nm) just below the sea surface ($\bar{Ed}_{PAR}$) for the Arabian Sea is determined from solar irradiance models and 7 years of satellite data (1979–1985). Model results of high spatial resolution (18 km) PAR distribution computed from actual monthly measurements (aerosols, cloud cover, and ozone) displayed small-scale patchiness that is not observed in PAR climatology models. Two elevated PAR periods are observed each year, as opposed to a single elevated period per year observed in the North Atlantic during the summer. When the biannual cycle for each of the 7 years is compared with the 7-year average, interannual changes in intensity and time are observed. Additionally, the PAR cycle is found to vary regionally within the Arabian Sea. The bimodal PAR distribution shows elevated peaks in May and October and minima in December (corresponding to the winter equinox) and July. The second minima occurs at the onset of the southwest monsoon, apparently in response to increased cloud cover and aerosols associated with the monsoon. This summer minima varied latitudinally. It originates in the southern regions (0°–10° latitude) in April and migrates north as the influence of the southwest monsoon moves northward, reaching the northern Oman coast (20° latitude) in August. Additionally, the summer minima is less pronounced as the southwest monsoon moves northward. Maximum PAR intensity is observed in early spring (preceding the minima), originating in the southern Arabian Sea and extending northward into the central Arabian Sea. The timing of the northward movement of this spring maximum is slightly different each year. The net yearly PAR intensity for each of the 7 years appears to remain approximately the same, despite the interannual variability in the cycle and regional variability. The timing and location of PAR cycles are important since they must be coupled with nutrient availability to understand biological cycles. We determined that for the Arabian Sea, PAR cycles determined by climatology may be inadequate to define the submarine light field and that high-resolution PAR cycles are needed to resolve realistic bio-optical and nutrient cycles.

1. Introduction

Approximately 47% of the total solar flux is received at the Earth's surface as incident short wave radiation (<700 nm). This short wave radiation is an essential parameter for marine photosynthesis and near-surface geochemical cycling. The amount of solar irradiance controls the rates of photosynthetic fixation of inorganic carbon to organic matter. This fundamental biological process governs the marine euphotic zone and couples processes taking place in the surface ocean with the global biosphere. As a result, knowledge of the short wave radiation distribution in the ocean is critical for understanding regional and temporal scales of the photosynthetic process. Because marine photosynthesis occurs in extremely short timescales (marine plant populations can double in 1 day) [e.g., *Shelton et al.*, 1972; *Goldman and McCarthy*, 1978], a knowledge of the short wave radiation distribution at the ocean surface at shorter spatial and temporal scales is required to assess the photosynthetic budget of a region.

Traditionally, we represent the solar irradiance at any depth in the euphotic zone as the photosynthetically available radiation (PAR), i.e., the short wave radiation integrated from 350 to 700 nm and representing light available to photosynthetic processes. PAR can both promote or inhibit the photosynthetic process and thus has a direct association with the phytoplankton growth and concentration in surface waters [*Arnone*, 1994; *Dickey and Simpson*, 1983]. Thus, PAR intensities regulate primary production in the euphotic zone through both photolimitation (too low) and photoinhibition (too high).

The subsurface light field and resulting vertical PAR distribution are a direct response to the intensity of incident solar irradiance flux entering at the sea surface. The vertical distribution of PAR in the euphotic zone is estimated by the attenuation of surface PAR by k_{PAR} (diffuse attenuation coefficient). The attenuation coefficient changes (spatially and temporally) with different water masses and is important in characterizing the submarine light field [*Sathyendranath et al.*, 1991]. However, the variability of PAR at the surface is perhaps more important in determining the subsurface light field

[1]Naval Research Laboratory, Stennis Space Center, Mississippi.
[2]Planning Sciences Incorporated, Slidell, Louisiana.
[3]Gulf Weather Corporation, Stennis Space Center, Mississippi.
[4]NOAA Coastal Service Center, Charleston, South Carolina.
[5]Severdrup Technology Inc., Stennis Space Center, Mississippi.

Paper number 97JC03204.
0148-0227/98/97JC-03204$09.00

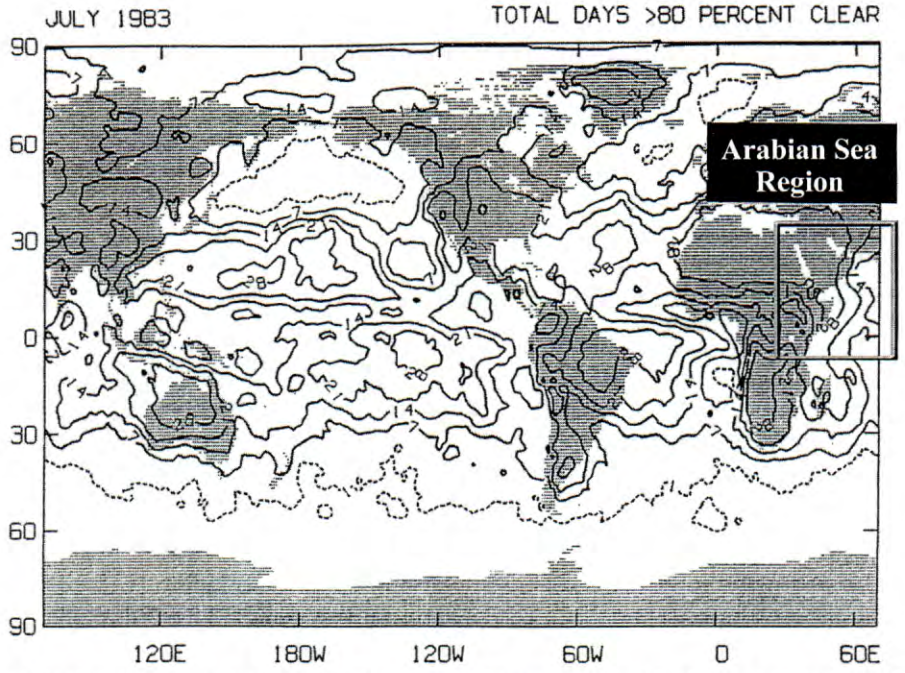

Figure 1. Solar irradiance contours do not show fine-scale spatial variability in the Arabian Sea [from *Bishop and Rossow*, 1991].

than changes in the water mass attenuation coefficient. The intensity of surface PAR therefore is a controlling parameter in the submarine light field and thus is a major factor in determining the primary production in the upper ocean. In this paper we will refer to PAR only at the ocean surface (Ed_{PAR}) and recognize that the vertical distribution is dependent on the attenuation coefficient. Our discussion focuses on the variability of the surface PAR intensity in the Arabian Sea and how it is distributed regionally and with time.

Besides being a controlling factor in the photosynthetic processes, the vertical distribution of this short wave radiation (350–700 nm) influences vertical subsurface heating rates [e.g., *Arnone et al.*, 1992a; *Dickey and Simpson*, 1983; *Siegel and Dickey*, 1986; *Lewis et al.*, 1990]. Of the total incoming radiation entering the ocean as short wave, less than 2% is absorbed for photosynthetic processes; the remainder is converted to heat [*Thurman*, 1988]. Long wave radiation is absorbed directly at the surface, and short wave radiation is differentially absorbed with depth and converted to heat, depending on the spectral nature of the submarine light field (spectral attenuation coefficient). Subsurface heating at different levels of the water column can lead to instabilities of surface waters. Most important, this subsurface heating is strongly linked to the regional and temporal distribution of surface PAR.

In addition to the seasonal cycle of the Sun, solar irradiance variability at the sea surface is influenced by atmospheric properties [*Bird*, 1984; *Arnone et al.*, 1993; *Gregg and Carder*, 1990]. Previous investigations have used cloud cover and the seasonal solar cycle to compute the solar irradiance distribution [*Bishop and Rossow*, 1991; *Brock et al.*, 1993] and have estimated solar irradiance for large ocean regions (280 km^2). Both results produce fairly uniform contours of surface irradiance (Figure 1) and do not represent the spatial, patchy nature of PAR that we will show is characteristic. This uniform smoothness may be the result of these studies, which did not include the aerosol influence in PAR intensity, or may be how PAR changes at the short spatial (18 km) scales or may determine how PAR intensities vary seasonally or yearly. Similarly, investigations of the aerosol variability in the Arabian Sea [*Husar et al.*, 1997] have illustrated large-scale changes but do not resolve the higher spatial or annual variability necessary for characterizing the PAR distribution.

Thus the scales of surface PAR used for climatological studies showing the distribution of surface PAR are limited in characterizing the submarine light field necessary for biological processes. Patchy phytoplankton concentrations have been observed in the open ocean under certain conditions that arise from the complex variation in light and nutrient availability and grazing, etc. [*Banse*, 1994]. Recent Arabian Sea observations of fine scales by towed underway systems, i.e., SeaSoar [e.g., *Weeks et al.*, 1997; B. Jones, personal communication, 1997], show this very clearly.

The biological response to light intensity and time exposure has been shown to strongly affect phytoplankton growth. In the North Atlantic, for example, the development of the spring bloom in April is primarily controlled by a coupled relationship between solar irradiance and nutrient availability [*Platt et al.*, 1991, 1992]. The North Atlantic solar irradiance cycle shows a single spring increase that reaches a maximum in midsummer and a decrease in fall [*Arnone et al.*, 1993]. During spring the system appears light-limited in the North Atlantic, and the bloom is triggered when light exposures reach a threshold level [*Dickey et al.*, 1993]. The decline of the bloom in summer appears to result from nutrient limitation and perhaps photoinhibition in surface waters.

In the Arabian Sea, aerosols from the African and Asian deserts are believed to have a significant role in controlling PAR distribution [*Brock et al.*, 1991]. *Husar et al.* [1997] has shown that the aerosol optical depths in the Arabian sea have the highest levels in the world ocean (depths >6.0). However, until now the spatial and temporal scales of PAR variability have been difficult to examine because of the limited amounts

of broad-area synoptic measurements. As a result, the spatial patchiness of the sea surface solar irradiance has not been well characterized, although it has been observed in high-resolution irradiance models [*Arnone et al.*, 1993; *Arnone*, 1994].

The Arabian Sea represents a region of exceptionally intense solar irradiance and elevated air and sea surface temperatures. Biological processes in the surface mixed-layer may be photoinhibited during several seasons, especially during the spring intermonsoon. These elevated surface PAR levels do not appear to adversely affect subsurface biological processes; even during the spring intermonsoon, primary production reaches a maximum in the pycnocline. The solar irradiance cycle in the Arabian Sea differs significantly from that of the North Atlantic due to the intermonsoonal periods (April and September) of maximum light intensity [*Brock et al.*, 1991, 1992, 1993, 1994; *Brock and McClain*, 1992; *Krey and Babeberd*, 1976]. Initial PAR models have characterized the mean solar irradiance distribution based on large-scale modeling over long time periods [*Brock et al.*, 1993; *Bishop and Rossow*, 1991; *Hastenrath and Lamb*, 1979]. However, the climatological PAR fields are clearly inadequate for resolving biological cycles occuring at the short timescales and spatial scales which are typically measured in ship collection programs. In a similar manner a comparison of numerical models forced by climatological and real-time winds shows very different results, indicating that real-time winds provide more realistic circulation patterns (J. Kindle, personal communication, 1997). We expect that a better characterization of the PAR distribution will improve our ability to understand biological cycles in the Arabian Sea. For example, slight changes in the annual timing of the monsoonal cycle and evolution across the Arabian Sea basin require that PAR spacescales and timescales be better refined.

In this paper the surface PAR cycle is described as it relates to the developing monsoon wind system. The monsoon cycle has different timing and intensities for different regions within the Arabian Sea. These spatial and temporal monsoonal variabilities have noticeable changes in the PAR cycle that are similarly highly variable. The monsoon cycle influences surface PAR distribution through modulation of the atmospheric transmission associated with aerosol distributions and cloud cover. Basically, the monsoonal system can be divided into four stages. The most intense winds of this cycle occur during the southwest monsoon cycle that originates in southern latitudes and migrates northward, reaching its full extent sometime in June as a major wind system (the Findlater jet) that affects much of the Arabian Sea [*Findlater*, 1966]. The southwest monsoon development evolves progressively in the basin. The southwest winds are most intense in the eastern basin off the Somali coast and diverge as they migrate westward toward India. These monsoonal winds diminish rapidly in September with the onset of the fall intermonsoonal period. In December the northwest monsoon begins with steady northeast winds that last until February. The winds of this monsoonal period are less intense than the southwest monsoon. The spring intermonsoon, from March through May, is characterized by reduced winds and variable directionality.

J. Kindle (personal communication, 1997) has shown that the interannual timing and intensity of these winds are far more variable in time and space than are indicated by the climatological winds such as described by *Hastenrath and Lamb* [1979]. This variability may be critical to forcing physical and biological processes and in changing atmospheric transmission (cloud cover and aerosols) that, in turn, affect the PAR cycle. For example, a stronger southwest monsoon may be inferred to yield more airborne dust and increased cross-equatorial moisture flux, yielding higher cloudiness over the Arabian Sea as the winds approach India. During any time period, as a result of this evolution, different regions in the sea will be at different developmental stages.

The objective of this paper is to define the spatial and monthly variability of PAR just below the ocean surface (Ed^-_{PAR}) for the Arabian Sea based on measured satellite-derived atmospheric properties and models. PAR cycles are characterized for different regions, and the interannual variation is examined. The development of PAR intensity is described in response to the monsoonal cycle as it progresses across the Arabian Sea basin, and the importance of timing within a region is demonstrated.

These realistic spatial and temporal considerations are needed to understand how the biological cycle and solar heating rates vary seasonally and regionally. While the influence of the monsoon cycle on the biophysical processes is not addressed in this paper, it should be noted that the surface bio-optical processes are coupled in response to both biophysical processes and the PAR cycle.

2. Model and Theory

The surface irradiance flux (W m^{-2}) is modeled to characterize the spatial and temporal variability using inputs of satellite data for 84 consecutive months (January 1979 through December 1985). The model is used to compute the solar irradiance spectrum from 350 to 700 nm just below the ocean surface (Ed^-_λ). The modeled irradiance flux (W m^{-2}) has been integrated to determine PAR and averaged over a 1-month period for 18-km grids.

The total solar irradiance ($Ed^+_{T\lambda}$) was computed as the sum of the direct ($Ed^+_{d\lambda}$) and the diffuse ($Ed^+_{s\lambda}$) components. The sea surface spectral irradiance model used here is a modified version of one developed by *Gregg and Carder* [1990]. Our version includes data input from satellite products of cloud cover estimates and aerosol optical depth measurements using monthly coastal zone color scanner (CZCS) data [*Bird*, 1984; *Terrie et al.*, 1992; *Arnone*, 1994].

The direct ($Ed^+_{d\lambda}$) clear-sky irradiance (i.e., the solar contribution) for a given wavelength is given by *Bird* [1984:

$$Ed_{d\lambda} += \cos(\Theta) F_{o\lambda} e^{\tau_{r\lambda}} e^{\tau_{a\lambda}} e^{\tau_{o\lambda}} e^{\tau_{w\lambda}} e^{\tau_{u\lambda}}, \quad (1)$$

where $F_{o\lambda}$ is the extraterrestrial spectral irradiance above the atmosphere; Θ is the solar zenith angle; and $e^{\tau_{r\lambda}}$, $e^{\tau_{a\lambda}}$, $e^{\tau_{o\lambda}}$, $e^{\tau_{w\lambda}}$, and $e^{\tau_{u\lambda}}$ are the optical depths of atmospheric transmission for Rayleigh scattering, aerosol extinction, ozone absorption, water vapor absorption, and uniformly mixed gas absorption, respectively (note that $e^{\tau_{w\lambda}}$ and $e^{\tau_{u\lambda}}$ are negligible in the spectral window between 350 and 700 nm). The aerosol transmittance ($\tau_{a\lambda}$) is obtained from historical CZCS radiances at 670 nm (La_{670}). The ozone optical thickness ($\tau_{O\lambda}$) obtained from the total ozone mapping spectrometer (TOMS) was collected coincidentally with the CZCS data at a spatial resolution of 50 km. The Dobson units from TOMS were converted to τ_O using values from the University of Miami [*McClain et al.*, 1992] and extrapolated across the spectral range. The spatial variability of $\tau_{O\lambda}$ is given by *Arnone et al.* [1993] for the North Atlantic; however, the contribution of $\tau_{O\lambda}$ is not a significant contribution to the direct ($Ed^+_{d\lambda}$).

2.1. Aerosol Optical Depth τ_a

Satellite-derived radiance in the "red" spectrum (670 nm) has been used to estimate the concentration of aerosols over oceanic regions and in atmospheric algorithms [*Gordon and Clark*, 1981]. (A similar approach has been used by *Husar et al.* [1997] in using the visible channel of the NOAA advanced very high resolution radiometer (AVHRR) to estimate the aerosol optical thickness.) Here we assume that water totally absorbs "red light" and that any radiance detected at satellite altitudes results from aerosol and Rayleigh scattering. Following removal of the Rayleigh scattering component, the La_{670} radiances represent the aerosol concentration. *Brown and Yoder* [1994] have shown that in specific ocean regions, coccolithophorid blooms can also contribute to the scattering at 670 nm and must be avoided. As they suggest, we limit valid La_{670} to values less than 1.10 mW cm^{-1} μm^{-1} to avoid erroneous contaminated aerosol values. *Haggerty et al.* [1990] have shown that radiance is related to optical thickness by

$$\mathrm{La} \approx \frac{\omega_o F_o}{4\mu} p(\Phi)\tau_{a\lambda}, \tag{2}$$

where La is the upwelling radiance due to aerosol scattering; τ_a is the optical depth due to aerosol scattering; ω_o is the single scattering albedo; $\mu = \cos(\theta)$, where θ is the solar zenith angle; $p(\Phi)$ is the scattering phase function, Φ is the scattering angle; and F_o is the incoming solar radiative flux. Here $p(\Phi)$ is estimated by a two-term Henyey-Greenstein function. The wavelength dependence of aerosol transmittance is related to the Angstrom coefficient η, where $\tau_{\lambda a}$ is extrapolated from the La_{670} channel of CZCS data:

$$\frac{\tau_{a670}}{\tau_{a\lambda}} = \left[\frac{\lambda}{670}\right]^{\eta}. \tag{3}$$

It is assumed that the aerosol scattering function is constant for a maritime atmosphere where $\eta = 0$. This assumes the scattering at 670 nm is directly proportional to the aerosol concentration and considers the aerosol particle to have a constant size, shape, and composition. We used the historical monthly averaged CZCS La_{670} over the Arabian Sea, which represents a spatial pixel of 18 km for 1979–1986 [*Feldman et al.*, 1989; *Arnone et al.*, 1992b]. Problems with CZCS calibration and sensor degradation with time are minimal for the 670-nm channels and were more serious for the shorter-wavelength channels. Since we are not using these channels, we believe our estimate of aerosol optical depth based on La_{670} is valid. Additionally, we are using the monthly average of the La_{670}. The difference between the maritime and continental atmosphere in these monthly averages could result in an error of only 3% of the total PAR intensity computed. We consider this to be within the variance of the computation and within the limits of the model computations. *Husar et al.* [1997] used the NOAA composite aerosol optical product from July 1989 to June 1991 to illustrate the spatial and temporal variability on a global basis at a 1° spatial resolution and 3-month average. Their Figure 1a of seasonal aerosol optical depth for the Arabian basin agrees with those derived with the basin composite CZCS La_{670} and confirm the importance of aerosols in this basin. We believe their spatial and temporal variability to be too coarse to resolve the PAR distribution required to address the biological response.

2.2. Influence of Clouds

The contribution of cloud cover was applied to both the direct ($Ed^+_{d\lambda}$) and diffuse ($Ed^+_{s\lambda}$) components. The cloud cover estimates are obtained from a real-time database using 3-hour observations during 1979–1986 [*U.S. Air Force*, 1986]. The direct component accounted for clouds according to $(Ed^+_{d\lambda})(1 - c)$, where c is percent cloud cover.

A simple model was employed to account for the effects of clouds by relating the diffuse irradiance (i.e., sky light irradiance) to percent cloud cover. According to *Lestrade et al.* [1990], the diffuse radiation ($E^+_{s\lambda}$) is 21% of total radiation on a cloud-free day; thus ($Ed^+_{d\lambda}$) from (1) is 79% of the total. For cloudy days, the percentage of diffuse radiation is Lestrade's equation (7):

$$h = 1.0 + 3.85c - 2.58c^2 \tag{4}$$

Since ($Ed^+_{d\lambda}$) is obtained from Equation (1), ($Ed^+_{s\lambda}$) can be expressed in terms of ($Ed^+_{d\lambda}$) as

$$Ed_{s\lambda} = 0.21 \frac{Ed_{d\lambda}}{0.79} h. \tag{5}$$

2.3. Subsurface Irradiance

The total solar irradiance at the ocean surface ($Ed^+_{\tau\lambda}$) is transmitted through the sea surface interface and extended to just below the surface (Ed^-_{λ}) [*Gregg and Carder*, 1990; *Koepke*, 1984] using

$$Ed^-_{\lambda} = Ed^+_{\lambda}(1 - R_{\lambda}) \tag{6}$$

where R_{λ} is the sea surface reflectance of both direct and diffuse and typically accounts for 2–4%. The surface direct and diffuse irradiance reflectances were subdivided into specular and reflectance components from sea foam. Fresnel reflectance was used to estimate specular reflectance and is dependent on the incident solar zenith angle, refracted angle, and wind speed [*Gregg and Carder*, 1990]. Foam reflectance was modeled after *Koepke* [1984] for a 4 m/s wind speed. We recognize that these wind speeds underestimate the seasonal variability of the speeds in this region (during the southwest monsoon 10 m/s); however, we expect only a minimal (<2%) influence on the subsurface PAR computed during these periods.

2.4. Photosynthetically Available Radiation

The modeled solar irradiance below the surface was computed at 10-nm spectral increments from 350 to 700 nm and integrated to estimate PAR just below the sea surface (Ed^-_{PAR}); the latter will be referred to as PAR.

3. Model Computation

The solar irradiance model was run at hourly time steps for each 18-km pixel location in the Arabian Sea, for each 10-nm wavelength, to compute the subsurface PAR just below the sea surface (Ed^-_{PAR}) for each month. The hourly solar position was used for each location to compute the direct and diffuse irradiance at the sea surface. Atmospheric inputs included monthly averaged values of aerosol optical depth and 3-day average values of ozone in computing the hourly irradiance. Additionally, the percent cloud cover for every 3-hour period was used. The daily irradiance flux below the surface was computed for each wavelength across the visible spectrum, and

then PAR was calculated. The monthly average was estimated from the daily averages beginning January 1979 through December 1985, or the life span of the CZCS satellite. Note that if the optical aerosol depth was not available from CZCS La_{670} data, then PAR was not computed at the given location. Typically, CZCS data were not available for periods when very high cloud cover occurred. However, this does not bias the computation. CZCS data are used only in the aerosol component of the direct irradiance component ($Ed^{+}_{d\lambda}$). The diffuse component ($Ed^{+}_{s\lambda}$) is the major component at high cloud cover, and this was computed based on the cloud cover database. Therefore the limitation of CZCS availability should not bias the PAR calculation. We elected not to estimate PAR for regions where an estimate of the aerosol transmittance was not available.

4. Results of the PAR Model

Examples of the 1979 monthly PAR computed from the model are illustrated in Plate 1 for January (northeast monsoon), May (spring intermonsoon), August (southwest monsoon), and November (fall intermonsoon). This sequence shows the regional variability of PAR in 1979 and how it changes seasonally. We will also show results of the PAR regional cycle for the other years to illustrate the interannual changes.

The 1979 PAR seasonal example illustrates both the seasonal latitude influence on PAR and the high, patchy nature of its spatial distribution. In January the PAR intensity decreases as we move to high latitudes. However, notice that in May just prior to the development of the southwest monsoon, the highest intensities occur in the central Arabian Sea and lower intensities occur along the equator, resulting from increased cloud cover. Patches of very high PAR (purple) are observed in the central Arabian Sea during this period. In August, after the southwest monsoon has begun, PAR becomes extremely variable as clouds and increased aerosol concentrations develop in the north. During this period the eastern basin shows a much lower PAR intensity than the western basin. By November we observe a separation of lower intensity in the eastern basin and a high PAR intensity in the western basin.

Interannual changes in PAR are seen by comparing the May data for 1979 and 1981 (Plates 1 and 2). Notice that in 1979, higher PAR intensities (browns and reds) are observed extending into the southern latitudes. In May 1981, significantly lower intensities (yellow) are observed in the southern equatorial regions as compared with 1979. This comparison indicates regional interannual PAR differences. Furthermore, it suggests that the PAR cycles and intensity levels may be associated with the interannual monsoon variability.

The results of the PAR model were initially averaged over the entire Arabian Sea for each month (entire region shown in Plate 1 excluding the Persian Gulf). The yearly PAR cycles over this region are shown for each year from 1979 to 1985 (Plate 3). (The Persian Gulf has distinctly different cycles, and we have refrained from including it in the Arabian Sea PAR average.) Missing data within the plot results when less than 1000 PAR values are computed for that month. We do not believe less than 1000 values adequately represent the PAR cycle. (For example, in 1985, no valid PAR values were computed for July, August, and September.) Consistently high PAR levels are observed in the spring. However, the intensity of these spring maxima are quite different from year to year, ranging from a high in 1983 (167 W m^{-2}) to a low in 1981 (144 W m^{-2}).

The midsummer decline in PAR intensity is also significantly different each year. In 1980 and 1981 the PAR intensity in June is lower than the winter period! This appears most unusual, since winter typically contains the month of minimal intensity in the northern hemisphere. Year-to-year changes in the aerosol distribution and cloud cover resulting from the monsoon are believed responsible for these differences in the PAR cycle. The maximum intensity is reached in spring (peaking in April) in all years except 1981, when low PAR levels were observed. Notice that in 1981 the summer minimum was very short and the fall maximum arrived early (this suggests a short southwest monsoon with little cloud cover and lower aerosol concentrations).

The average PAR cycle of the entire basin for 1979–1985 is presented in Plate 4 as PAR climatology. The PAR pattern in the figure is similar to that of *Brock et al.* [1993], with elevated PAR intensity (155 W m^{-2}) in April and a second elevated PAR intensity in September (140 W m^{-2}). However, note that the climatological PAR cycle in this plate is quite different from that observed for any particular year in Plate 3. The PAR cycle can be linked with *Husar et al.*'s [1997] aerosol optical thickness for the Arabian Sea. Their increases in aerosol optical thickness (>6.0 in their Figure 1a) are shown to occur during the SW monsoon, which corresponds to our computed decrease in PAR intensities. Although showing similar trends, the aerosol optical depth derived from the CZCS that we used to describe the spatial and temporal variability clearly identified details of the timing of the monsoon and the subbasin changes that are not observed in the AVHRR aerosol product.

The difference of the PAR climatology with a specific year's monthly average is identified as the residual PAR in Plate 5. The significant changes in timing and intensity observed in Plate 5 indicate inadequacies of applying multiyear averages to characterize the PAR cycle. Notice that in May 1983 a strong positive anomaly occurs, resulting from abnormally high PAR. This positive anomaly may have been associated with the El Niño–Southern Oscillation (ENSO) event that occurred during this time. Predictions have indicated that during an Indian Ocean El Niño, the southwest monsoon is weaker and less moisture is advected over India [*Eos*, 1994]. This reduced cloud cover would enhance the PAR intensity and account for the elevated levels that were observed.

We have summed the residuals for all months for each year and report the cumulative change from year to year in Table 1. Positive values indicate a net gain in PAR intensity from the mean. Note that the differences in the yearly residuals are quite small, indicating the total short wave energy available to the basin is fairly constant, and that it is how the energy is spatially distributed within the monthly cycle that is important.

4.1. Regional PAR Variability

The regional variability of the PAR cycle was characterized for seven regions that have different ocean processes (Plate 6). The first is the Persian Gulf, a region with minimum monsoonal influence and elevated sea surface and air temperatures. The second is the Gulf of Oman, which has little monsoonal influence in the region of mixing of Arabian Sea and Persian Gulf waters. Third is the Oman coastal region, which has upwelling along the coast during the southwest monsoon and development of filaments extending into the central Arabian Sea. Fourth is the Indian coastal region. As the Findlater jet extends across the Arabian Sea basin to the coast of India,

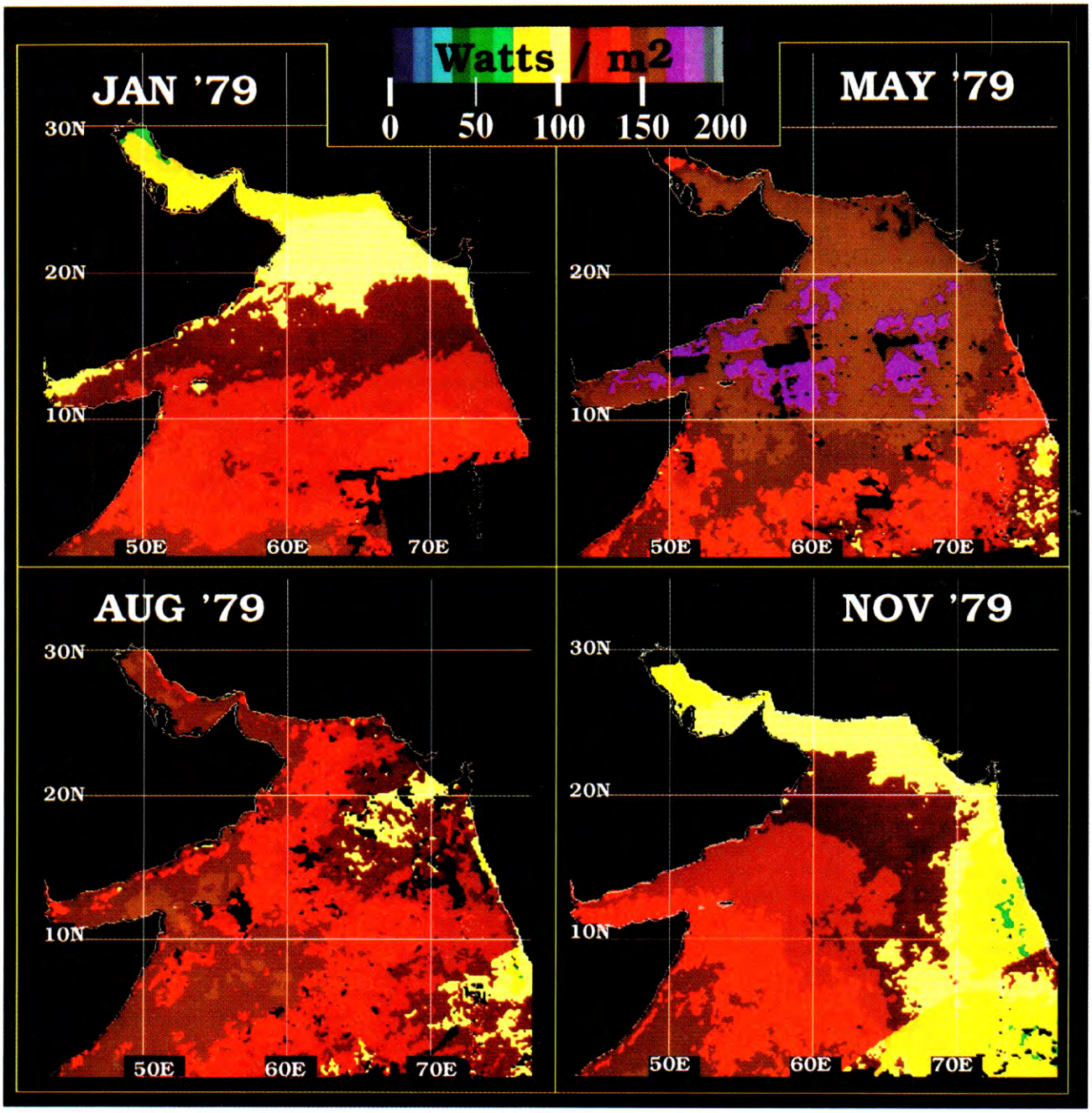

Plate 1. Examples of modeled photosynthetically available radiation (PAR) intensity just below the surface (Ed^-) in the Arabian Sea for 1979: (a) January (northeast monsoon), (b) May (spring intermonsoon), (c) August (southwest monsoon), and (d) November (fall intermonsoon).

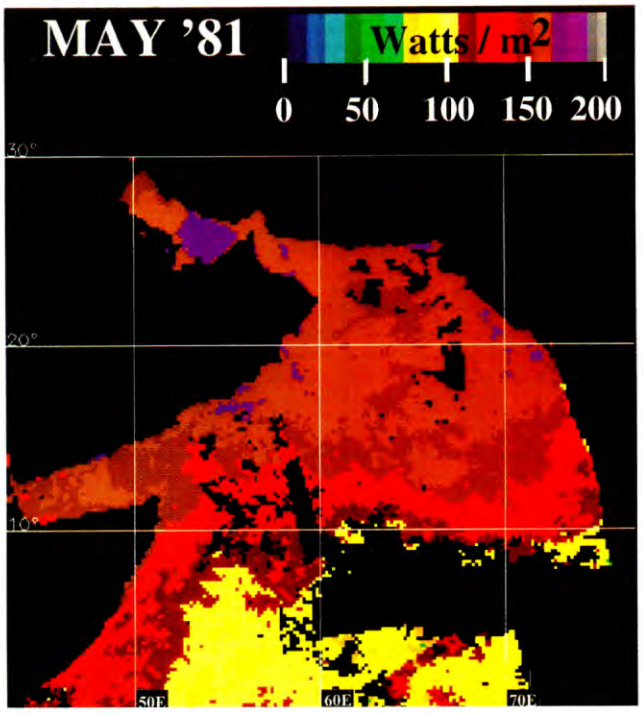

Plate 2. PAR variability for May 1981. Compare with May 1979 (Plate 1) for the Arabian Sea basin.

it picks up moisture and produces increased cloud cover during the southwest monsoon. Fifth is the Somali upwelling region. The western basin is influenced by the intense winds of the Findlater jet and intense coastal upwelling. Sixth is the central north Arabian Sea. The central basin is influenced by atmospheric and oceanic mesoscale circulation and is disassociated from coastal effects. Last is the equatorial region, which represents excessive cloud development of the Intertropical Convergence Zone and the origins of the monsoon.

Two-week-average wind speeds at each of these regions were computed from the numerical weather prediction models of the European Centre for Medium-Range Weather Forecasts (ECMWF) models and are presented for 1981 (Plate 7a). The wind speed structure shows the onset of the southwest monsoon beginning in late May and June that is responsible for changes in the atmospheric transmission structure (aerosols and cloud cover). We observed a difference in the timing of the winds and the magnitude for these regions. The southwest monsoon begins in late May in the Somalia region, where the winds are the greatest, and begins in the Indian coast region in mid-June. The relationship of the 1981 wind speed with PAR intensity is shown for the central Arabian Sea region (Plate 7b). Notice that PAR intensity decreases rapidly as the southwest monsoon begins in June and indicates that the PAR cycle is coupled to the monsoon cycle.

The PAR cycle for each of these regions is shown for years 1979–1985 (Plates 8a–8g), illustrating the interannual changes in each of these areas. The 7-year averages for each region are shown in Plate 8h, illustrating differences in timing of the PAR cycle. (Because of unavailable aerosol data from CZCS due to insufficient coverage, PAR was not computed for certain locations and time periods and accounts for missing data in the plot.) The northern regions (Plates 8a–8d) all show a minimum occurring in December and January, with a steady PAR increase extending into the spring transition period. In comparison, PAR cycles in southern regions appear to lead the northern regions by 1–2 months, depending on location.

The most noticeable difference in the PAR cycle for all regions except the Persian Gulf occurs in the summer months. The Persian Gulf region (Plate 8a) shows a cycle similar to that of the North Atlantic [*Arnone et al.*, 1993] and is quite different from the other Arabian Sea regions. This region shows an increase in PAR with a maximum in summer, followed by a decrease in fall, and does not experience a monsoon climate; i.e., neither in winter nor summer does the monsoon airflow reach this far north. As we move southward into the Gulf of Oman (Plate 8b), a noticeable decrease occurs in PAR intensity in midsummer (July). Farther south in the Oman coast region of the northern Arabian Sea (Plate 6c), the decrease is more pronounced through June with a slight increase in September.

In the eastern basin along the Indian coast (Plate 8d) the influence of the monsoon is more apparent, as a decrease in PAR intensity is clearly observed in midsummer (July). A strong PAR increase in spring is consistent from year to year, reaching a maximum in May. However, the summer decline in July is highly variable from year to year. Notice that in 1980, July PAR intensity is lower than the winter equinox in December.

In the Somali upwelling region (Plate 8e), PAR intensity is consistently high throughout the year. The PAR cycle, however, appears dampened, possibly resulting from increased fog and high aerosols associated with this region. The maximum PAR intensity that occurs in spring is variable from year to year. Notice the unusually low 1981 PAR levels when a spring maximum did not occur. In this region the summer PAR decrease is long and begins early in May and lasts until September. This region's cycle precedes the climatological PAR cycle (Plate 3) by several months. The Somali upwelling becomes active prior to the upwelling off Oman as the monsoon develops in the southwest. This can possibly account for the early PAR maximum in this region.

The central Arabian Sea (Plate 8f) shows the development of the PAR spring maximum (April), followed by the summer minimum in June. Note the interannual variability in time and intensity is substantial in this region, especially in the late summer (July, August, September). For example, in 1981 the summer minimum occurred in June, compared with July in 1979. This region's summer PAR minimum represents approximately a 1-month delay from the Somali region. We also note summer intensities are lower than winter for 1980 and 1981, a pattern similar to that observed in the Indian coastal region.

The equatorial region (Plate 8g) shows PAR intensity lower than expected at this latitude. This region shows the greatest interannual variability of the PAR cycle for any region, and it is very difficult to define a definite PAR cycle. The summer months show the lowest PAR intensities for any region (<100 W m^{-2}). The spring maximum shows substantial differences in 1980, 1981, and 1983. The average PAR cycle shows a long period of low PAR values extending from April to September and is the longest of any cycle.

The 7-year average PAR cycle for each region is shown in Plate 8h. We observe regional differences of 90% that occur in the winter months. Regional differences also occur in summer PAR intensities that are believed associated with changes in monsoonal intensity. Lowest PAR intensities are observed for (1) equatorial, followed by (2) Indian coast, (3) central Arabian Sea, (4) Somalia upwelling, (5) Oman coast, and (6) Gulf of Oman.

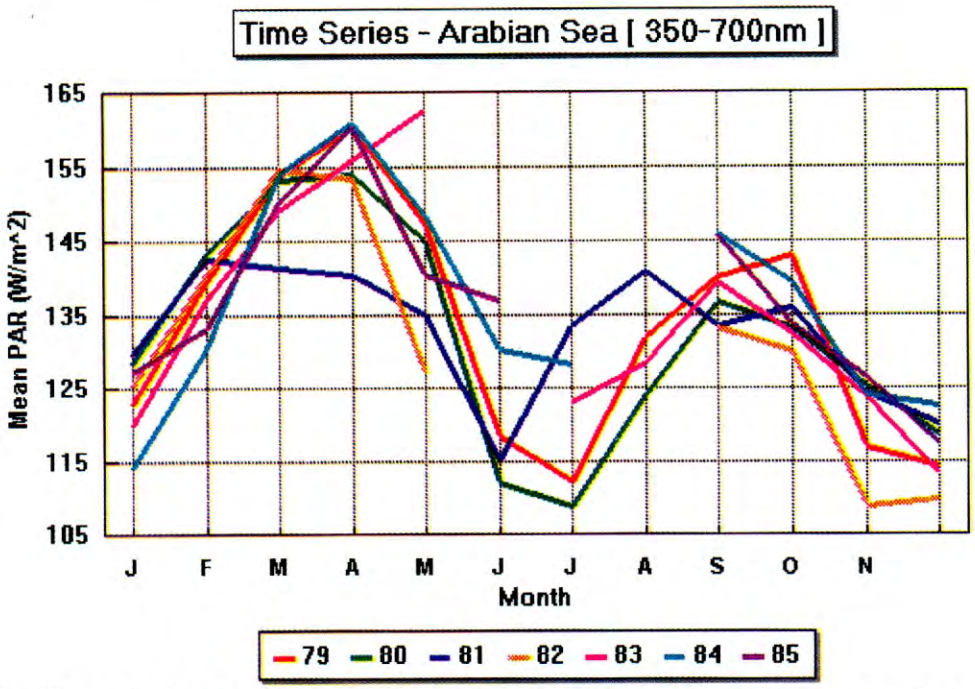

Plate 3. Changes in the annual PAR cycle from 1979 to 1985 for the entire Arabian Sea basin (omitting the Persian Gulf) shown for monthly averages.

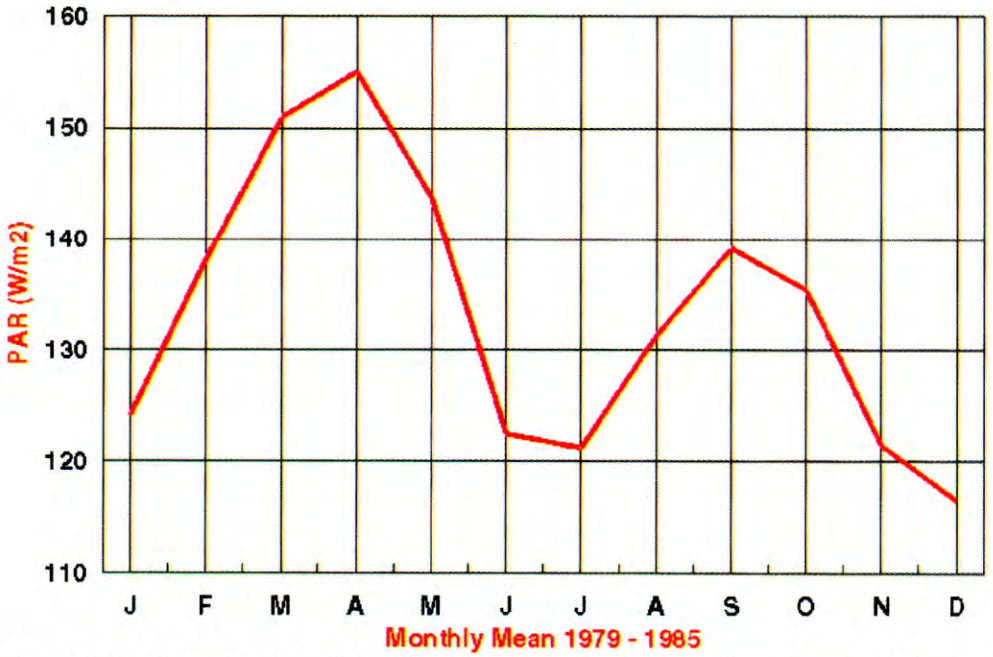

Plate 4. The mean interannual PAR intensity at the sea surface for the entire Arabian Sea basin (excluding the Persian Gulf and the Red Sea region) from 1979 to 1985 (note similarity with *Brock et al.* [1993]).

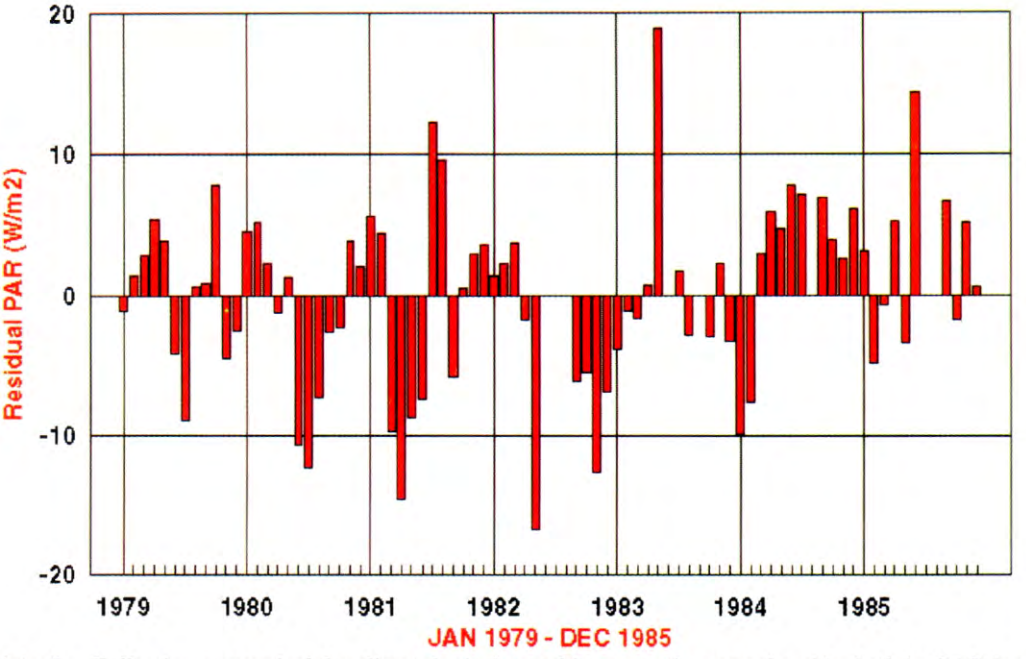

Plate 5. Following removal of the climatological monthly mean, the annual residual of the PAR intensity is shown for 1979–1985.

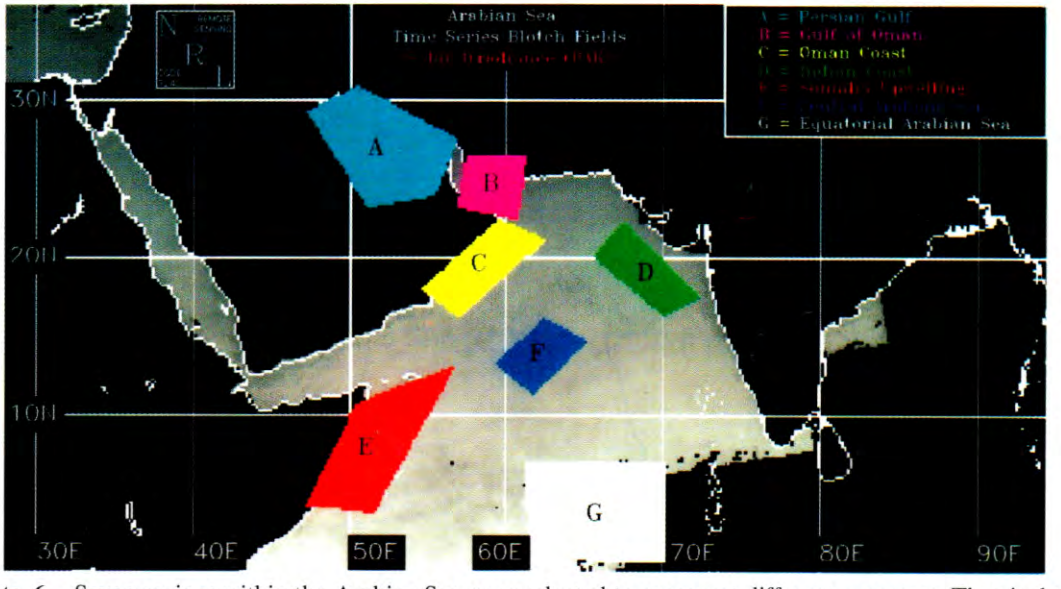

Plate 6. Seven regions within the Arabian Sea were selected to represent different processes. They include (a) Persian Gulf, (b) Gulf of Oman, (c) Oman coast, (d) Indian coast, (e) Somali upwelling, (f) central Arabian Sea, and (g) equatorial.

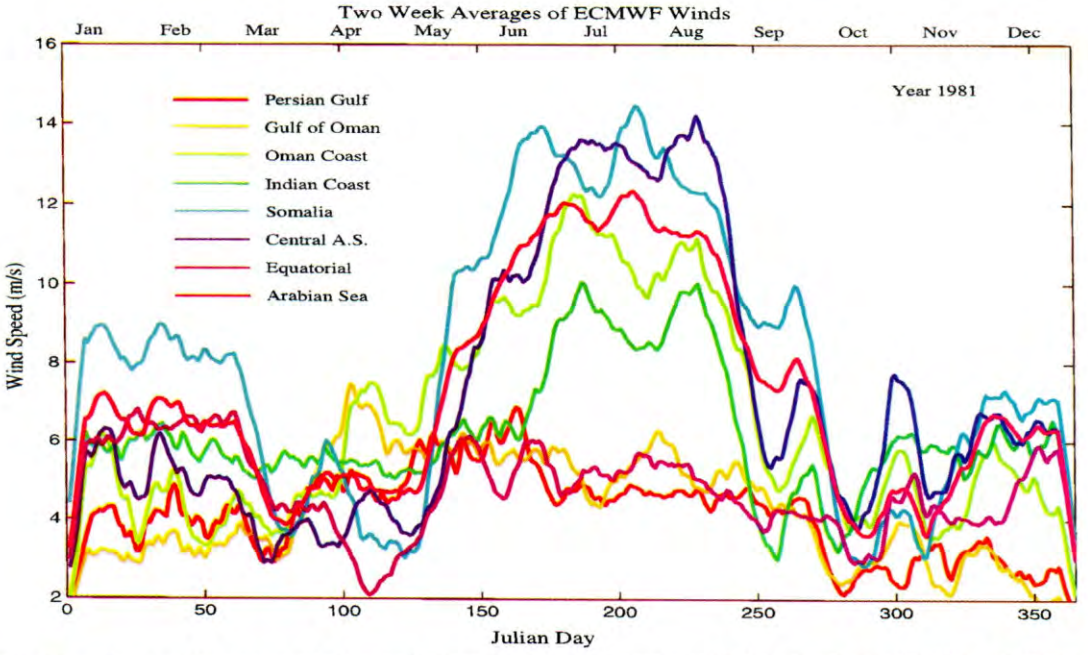

Plate 7a. Two-week average wind magnitudes for the seven regions in Plate 6 are shown for 1981. Notice the differences in timing and magnitude of the southwest monsoon (June–July) that occur for these regions.

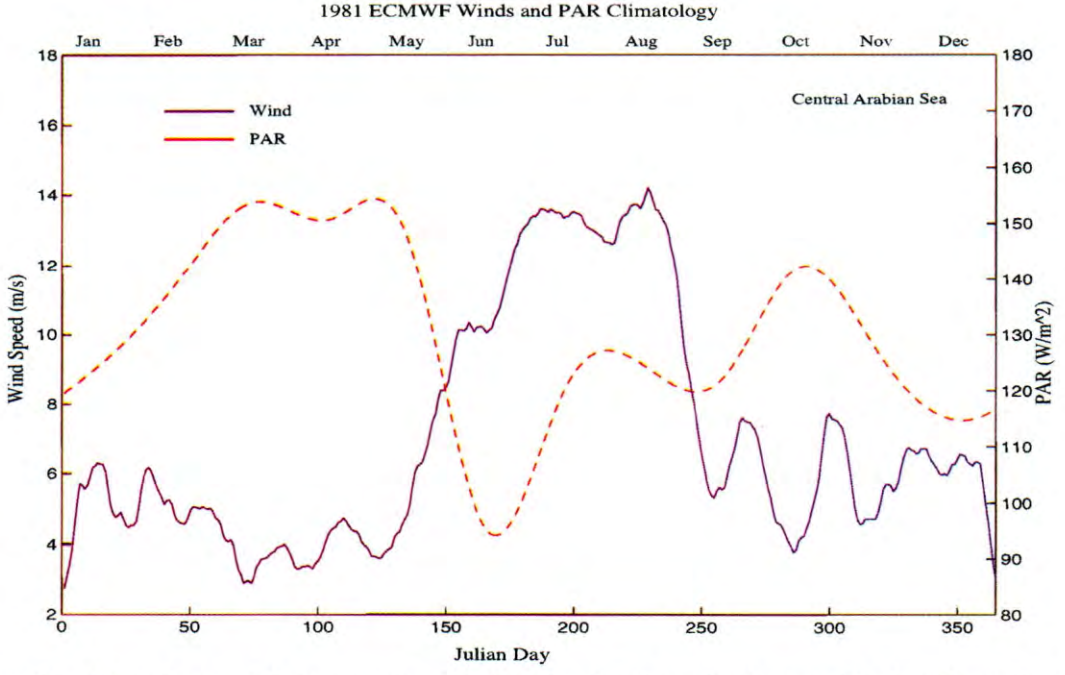

Plate 7b. The influence of the monsoon cycle on PAR levels is shown for the central Arabian Sea region for 1981. Increased wind magnitudes in June show a coincident decrease in PAR intensity.

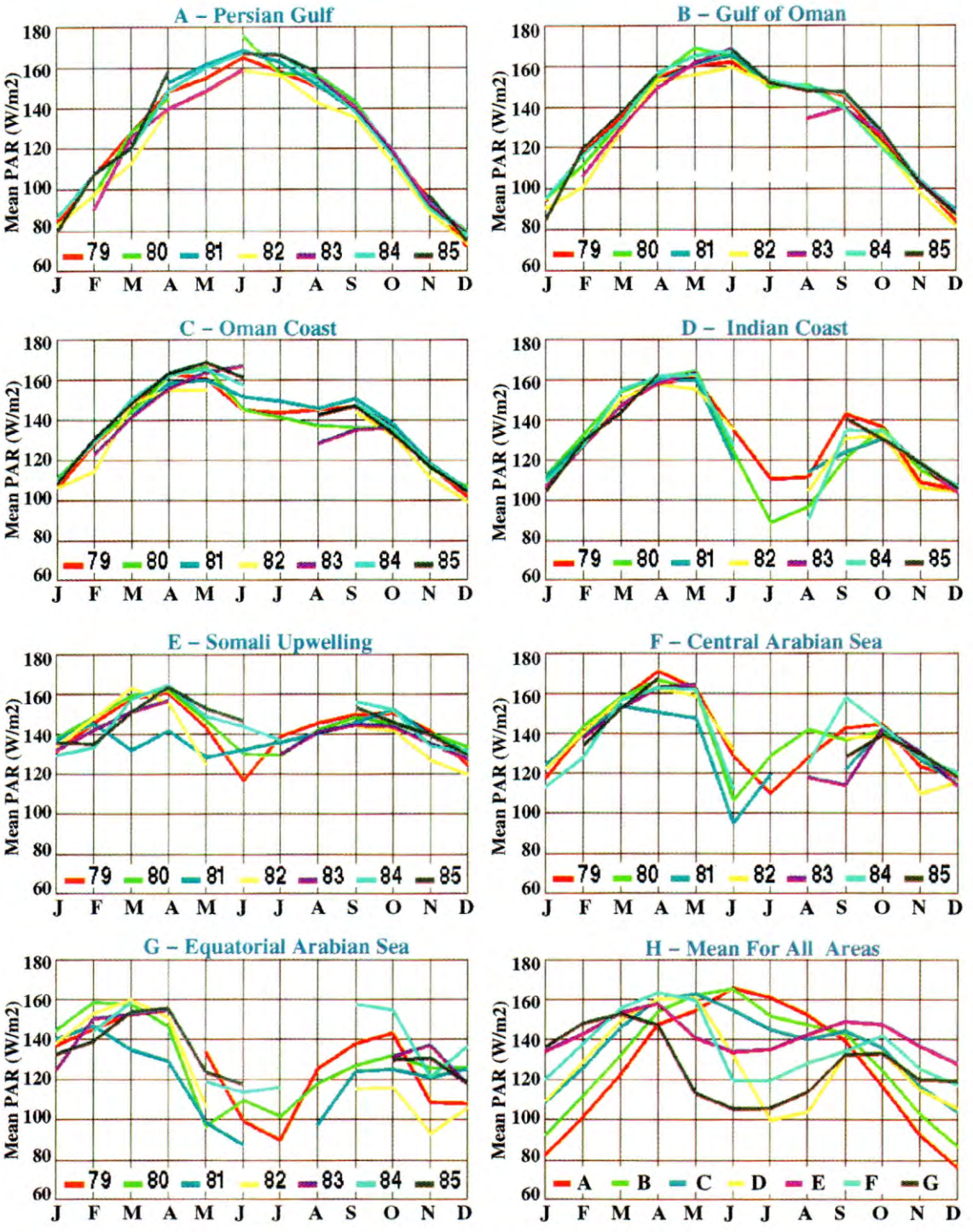

Plate 8. The monthly PAR cycles for the seven regions in Plate 6 are different. For each region the interannual cycle is shown from 1979 to 1985. The northern and eastern regions (Plates 8a–8d) have higher PAR intensity during the summer months than the western and southern regions (Plates 8e–8f). The 7-year monthly PAR average for each of the regions is shown in Plate 8h.

Table 1. Changes in Yearly Total of PAR From PAR Climatology

Year	Annual Residual, W m^{-2}
1979	1.8
1980	−17.0
1981	−7.1
1982	−41.7
1983	8.6
1984	30.6
1985	24.9

Positive values indicate a net gain in photosynthetically available radiation (PAR) intensity from the mean. Note that the differences in the yearly residuals are quite small, indicating the total short wave energy available to the basin is fairly constant, and that it is how the energy is spatially distributed within the monthly cycle that is important.

4.2. PAR Variability With Latitude

Because of the obvious latitudinal effect of PAR intensity within the Arabian Sea basin, we calculated a latitudinal average for each 1° for each month for the period 1979–1985 in Plate 9. (This plate averages the east-west effects of the PAR model in the basin and defines the latitudinal influence on PAR.) The latitude average is plotted for each month. By selecting a latitude in Plate 9, the monthly PAR cycle can be determined across the time (x) axis.

Maximum (red) PAR intensity is observed each year in spring, with a secondary peak (yellow) in fall. Minimum PAR intensity (blue) occurs in December and in midsummer (June). Black areas on this plot occur where PAR was not computed because the monthly average aerosol data from CZCS were not available. These periods usually occur when high cloud cover limited CZCS data collection and therefore represents periods of very low PAR intensity.

The year-to-year variability of these intensities in the 7-year period reemphasizes our thesis that investigators must use caution when using PAR climatology to characterize the regional light field. The interannual north-south migration of the summer minimum PAR is detectable in Plate 9. Spring maximum PAR (red) originates at low latitudes in February. This maximum PAR migrates northward each month, reaching 25° north latitude approximately in June. More important, the minimum PAR intensities (blue) in midsummer, a result of the southwest monsoon's increased cloud cover, originate at low latitudes (<5°) in April and extend northward, affecting the PAR intensity. This midsummer PAR minimum is variable each year and is undoubtedly a direct response to the changes in the monsoon.

Notice that in Plate 9 a ridge of high PAR is observed between 13° and 15° north latitude in the central Arabian Sea during summer (April–August). Lower intensities occur both to the north and south of this ridge. The ridge is clearly defined in 1981 at 14°–15° north; however, characteristics of this same feature are observed in other years. PAR cycles north and south of this ridge are shown to have a strong minimum occurring during the summer months. This latitudinal minimum is observed in August 1979 (Plate 1c) when a noticeable decrease (yellow) is observed in the western basin at 18°–20° north. Plate 1c shows that higher intensities are observed in the western basin and at lower latitudes (at approximately 13° north latitude). The decrease in PAR in the eastern basin at 18° north results from the accumulation of moisture as the Findlater jet propagates eastward over the Arabian Sea basin. Cloud and moisture development are highly variable in the eastern basin and are directly coupled to the monsoon variability and reduced PAR intensity.

5. Conclusions

We have defined the spatial and temporal variability of PAR just below the sea surface in the Arabian Sea from 1979 to 1985 through the use of a high-resolution model. These results are important for defining how changes in the surface light field can influence biological growth and primary production. We

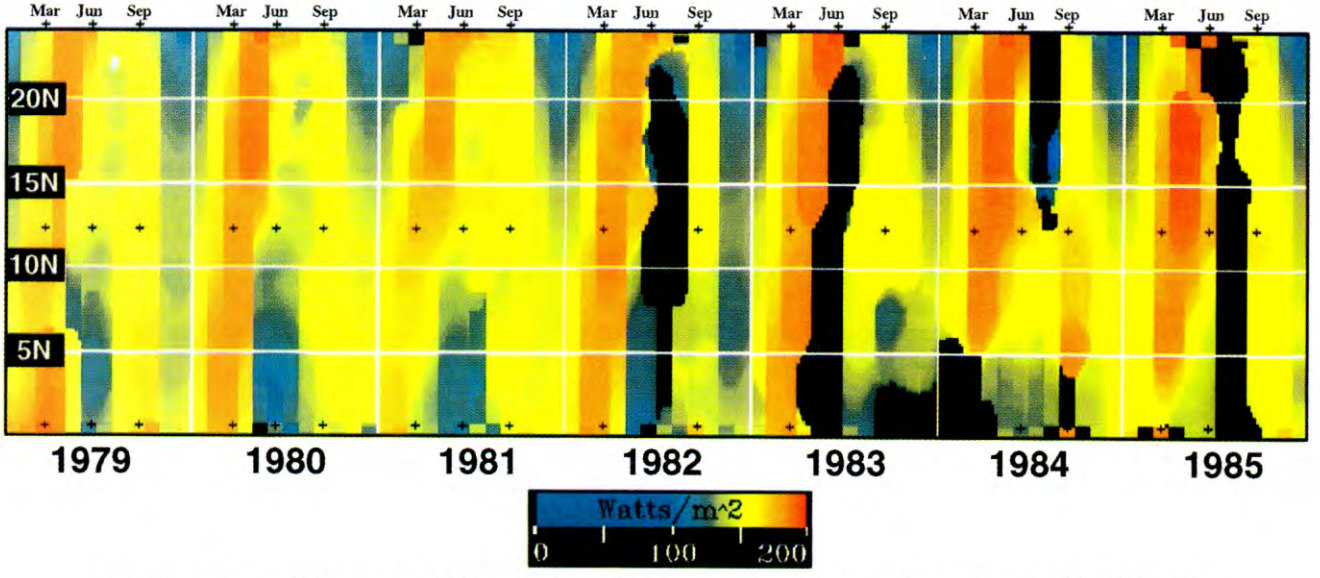

Plate 9. The monthly average PAR intensity for each degree of latitude is shown from 1979 to 1985. The annual spring maximum PAR (red) is shown advancing from low to high latitudes from March to June. The annual summer minimum PAR (blue) is shown responding to the onset of the southwest monsoon.

modeled the monthly averaged PAR using input from satellite-derived measurements of aerosols, ozone, and cloud cover. Monthly PAR was computed at 18-km resolution at hourly time steps and accounted for latitudinal influence on solar radiation. These results suggest that previous PAR models that are based on climatological input and limited aerosol input do not characterize the regional and temporal variability of the PAR cycle.

Our modeled results of monthly conditions indicate a biannual cycle of PAR showing a maximum peak in spring and a secondary peak in fall. However, the timing of this cycle is different throughout the Arabian Sea and varies in intensity from year to year. We have determined the 7-year average of PAR over the entire Arabian Sea and compared this average with individual years within this period and have observed significant differences.

In essence, we have found that during the southwest monsoon a decrease in PAR intensity is observed that appears variable in both intensity and timing and is probably related to monsoonal variability. We show that the typical PAR cycle changes substantially in different regions. Both the intensity and timing of the cycle change with latitude and within the eastern and western basin. Southern regions (equatorial) show a more pronounced and longer minimum in May and June than those in the north. This PAR minimum has lower intensities in summer periods than in winter when solar angles are low. A similar PAR cycle is observed in the central Arabian Sea and in the western basin. In the northern regions and along the Oman coast, the summer PAR minimum is noticeably different. PAR intensity peaks in June in the Persian Gulf (25° latitude) and does not show a midsummer decrease. Along the Oman coastal region the PAR cycle peaks several months earlier (April or May) and is followed by a decrease in June and July. The interannual variability of this cycle can shift by 1 or 2 months, depending on the strength of the southwest monsoon during any single year.

The subsurface PAR cycle can influence the surface phytoplankton distribution and primary production. In the northern Arabian Sea the strong phytoplankton bloom that occurs during the southwest monsoon in July–August [*Brock et al.*, 1992; *Brock and McClain*, 1992] follows the PAR minimum in June–July. The southwest monsoon influences both the PAR cycle (through increased cloud cover and variable atmospheric conditions) and nutrient distribution (by advection and mixing processes). If we are to understand the dynamics of the primary production and phytoplankton distribution, the submarine light field must be characterized both spatially and temporally. These results indicate that the surface distribution of the light field is highly variable, and we expect the subsurface light field will have a similar variability, although we have not presented the variability of the attenuation coefficient.

Simply defining average PAR climatology appears insufficient for determining regional intensities and timing cycles needed to understand the phytoplankton blooms and primary production in the Arabian Sea basin. We consider the PAR cycle an important process for characterizing biophysical processes. High spatial and temporal resolution models of PAR are required to determine the surface and subsurface light field.

Acknowledgments. The authors thank P. Martinolich, S. Oriol, and G. Terrie for software development of the PAR model and for help in data processing. Additionally, appreciation is extended to Goddard Space Flight Center for the CZCS and TOMS data and to the NOAA Data Climatic Center for the cloud cover data. Appreciation is extended to T. Dickey and anonymous reviewers for comments that greatly improved the manuscript. Special thanks are extended to J. Kindle for wind data. This project was funded by the Naval Research Laboratory 6.1 program Forced Upper Ocean Dynamics, project element 601153.

References

Arnone, R. A., The temporal and spatial variability of chlorophyll in the western Mediterranean, in *Seasonal and Interannual Variability of the Western Mediterranean Sea*, *Coastal Estuarine Stud.*, vol. 46, edited by P. La Violette, pp. 195–225, AGU, Washington, D. C., 1994.

Arnone, R. A., G. E. Terrie, and P. J. Martin, Dependence of ocean heating on the distribution of spectral irradiance in the North Atlantic, in *Optics of the Air-Sea Interface*, edited by L. Estep, *Proc. Soc. Photo-Opt. Instrum. Eng.*, *1749*, 73–82, 1992a.

Arnone, R. A., R. A. Oriol, G. E. Terrie, and L. Estep, Ocean optical database, *NRL Tech. Note 254*, Nav. Res. Lab., Stennis Space Center, Miss., May 1992b.

Arnone, R. A., G. E. Terrie, and R. A. Oriol, Relationships between surface chlorophyll and solar irradiance in the North Atlantic, *Mar. Technol. Soc. J.*, *27*(1), 16–23, 1993.

Banse, K., On the coupling of hydrography, phytoplankton, zooplankton and settling organic particles offshore in the Arabian Sea, *Proc. Indian Acad. Sci.*, *103*(2), 125–161, 1994.

Bird, R. E., A simple solar spectral model for direct-normal and diffuse horizontal irradiance, *Sol. Energy*, *32*, 461–471, 1984.

Bishop, J. K. B., and W. B. Rossow, Spatial and temporal variability of global surface solar irradiance, *J. Geophys. Res.*, *96*(C9), 16,839–16,858, 1991.

Brock, J. C., and C. R. McClain, Interannual variability in phytoplankton blooms observed in the northwestern Arabian Sea during the southwest monsoon, *J. Geophys. Res.*, *97*(C1), 733–750, 1992.

Brock, J. C., C. R. McClain, M. E. Luther, and W. W. Hay, The phytoplankton bloom in the northwest Arabian Sea during the southwest monsoon of 1979, *J. Geophys. Res.*, *96*(C11), 20,623–20,642, 1991.

Brock, J. C., C. R. McClain, and W. W. Hay, A southwest monsoon hydrographic climatology for the northwestern Arabian Sea, *J. Geophys. Res.*, *97*(C6), 9455–9465, 1992.

Brock, J., S. Sathyendranath, and T. Platt, Modeling the seasonality of submarine light and primary production in the Arabian Sea, *Mar. Ecol. Prog. Ser.*, *101*, 209–221, 1993.

Brock, J., S. Sathyendranath, and T. Platt, A model study of seasonal mixed-layer primary production in the Arabian Sea, *Proc. Indian Acad. Sci.*, *103*(2), 163–176, 1994.

Brown, C. W., and J. A. Yoder, Coccolithophorid blooms in the global ocean, *J. Geophys. Res.*, *99*(C4), 7467–7482, 1994.

Dickey, T., and J. J. Simpson, The influence of optical water type on the diurnal response of the upper ocean, *Tellus*, *Ser. B*, *35*, 142–154, 1983.

Dickey, T., et al., Seasonal variability of bio-optical and physical properties in the Sargasso Sea, *J. Geophys. Res.*, *98*(C1), 865–898, 1993.

Eos, Indian Ocean may have El Nino of its own, *Eos Trans. AGU*, *75*(50), 585–586, 1994.

Feldman, G., W. G. Esaias, C. McClain, R. Evans, O. Brown, and J. Elrod, Ocean color: availability of the global data set, *Eos Trans. AGU*, *70*(23), 643, 1989.

Findlater, J., Cross-equatorial jet stream at low level over Kenya, *Meteorol. Mag.*, *95*, 353–364, 1966.

Goldman, J. C., and J. J. McCarthy, Steady state growth and ammonium uptake by a growing marine diatom, *Limnol. Oceanogr.*, *22*, 932–936, 1978.

Gordon, H. R., and D. K. Clark, Clear water radiance for atmospheric correction of coastal zone color scanner imagery, *Appl. Opt.*, *20*(24), 4175–4180, 1981.

Gregg, W. W., and K. L. Carder, A simple spectral solar irradiance model for cloudless maritime atmosphere, *Limnol. Oceanogr.*, *35*(8), 1656–1675, 1990.

Haggerty, J. A., P. A. Durkee, and B. J. Wattle, A comparison of surface and satellite-derived aerosol measurements in the western Mediterranean, *J. Geophys. Res.*, *95*(C2), 1547–1557, 1990.

Hastenrath, S., and P. Lamb, *Climatic Atlas of the Indian Ocean*, vol. 1, *Surface Circulation and Climate*, 109 pp., Univ. of Wisc. Press, Madison, 1979.

Husar, R. B., J. M. Prospero, and L. L. Stowe, Characterization of tropospheric aerosol over the ocean with the NOAA advanced very high resolution radiometer optical thickness operational product, *J. Geophys. Res.*, *102*(D14), 16,889–16,909, 1997.

Koepke, P., Effective reflectance of oceanic whitecaps, *Appl. Opt.*, *23*, 1816–1824, 1984.

Krey, J., and M. Babeberd, *Phytoplankton Production Atlas of the International Indian Ocean Expedition*, Inst. fur Meereskunde an der Univ. Kiel, Kiel, Germany, 1976.

Lestrade, J. P., B. Cock, and T. Trent, The effect of cloud layer plane albedo on global and diffuse insolation, *Sol. Energy*, *44*, 115–121, 1990.

Lewis, M. R., M. E. Carr, G. Feldman, C. McClain, and W. Esaias, Influence of penetrating solar radiation on heat budget on the equatorial Pacific Ocean, *Nature*, *347*, 543–545, 1990.

McClain, C. R., G. Fu, M. Darzi, and J. K. Firestone, PC-SeaPAk users' guide, *NASA Tech. Memo. 104557*, 105 pp., 1992.

Platt, T., C. Caverhill, and S. Sathyendranath, Basin-scale estimates of oceanic primary production by remote sensing: The North Atlantic, *J. Geophys. Res.*, *96*(C8), 15,147–15,159, 1991.

Platt, T., S. Sathyendranath, O. Ulloa, W. G. Harrison, N. Hoeffner, and J. Goes, Nutrient control of phytoplankton, photosynthesis in the North Atlantic, *Nature*, *356*, 229–231, 1992.

Sathyendranath, S., A. D. Gouveia, S. R. Shetye, P. Ravindran, and T. Platt, Biological control of surface temperature in the Arabian Sea, *Nature*, *349*, 54–56, 1991.

Siegel, D. A., and T. D. Dickey, Variability of net longwave radiation over the eastern north Pacific Ocean, *J. Geophys. Res.*, *91*(C6), 7657–7666, 1986.

Shelton, R. W., A. Prakash, and W. H. Sutcliffe Jr., The size distribution of particles in the ocean, *Limnol. Oceanogr.*, *17*, 327–340, 1972.

Terrie, G., R. A. Arnone, and R. A. Oriol, Variability of solar irradiance at the ocean surface, in *Optics of the Air-Sea Interface*, edited by L. Estep, *Proc. Soc. Photo-Opt. Instrum. Eng.*, *1749*, 37–48, 1992.

Thurman, H. V., *Introduction to Oceanography*, 7th ed., 515 pp., Macmillan, New York, 1988.

U.S. Air Force Environmental Technical Applications Center, Real time nephanalysis: USAFETAC climatic database users handbook 1, *USAFETAC/UH86/001*, Scott Air Force Base, Ill., 1986.

Weeks, A., D. Ballestero, and I. Robinson, Optical properties of the upper ocean in the Arabian Sea in August 1994, in *Ocean Optics XIII*, edited by S. G. Ackleson and R. Frouin, *Proc. Soc. Photo-Opt. Instrum. Eng.*, *2963*, 570–578, 1997.

R. A. Arnone, Naval Research Laboratory, Code 7343, Stennis Space Center, MS 39529. (e-mail: arnone@nrlssc.navy.mil)

J. C. Brock, NOAA Coastal Service Center, 2224 South Hobson Avenue, Charleston, SC 29405-2413.

S. Ladner, Planning Sciences Incorporated, 115 Christian Lane, Slidell, LA 70458.

P. La Violette, Gulf Weather Corporation, Stennis Space Center, MS 39529.

P. A. Rochford, Severdrup Technology Inc., Stennis Space Center, MS 39529.

(Received September 17, 1996; revised July 9, 1997;
accepted September 16, 1997.)